Chapter 8

Interaction of a vortex with other vortices

In a system of many vortices, such as a vortex tangle in Helium II or a vortex lattice in Helium II and dilute BECs, it is the interaction between vortices, rather than the density inhomogeneity, that dominates the dynamics of the system. At relatively large temperatures, thermal dissipation is the dominant dissipation mechanism of the vorticity. However, at very low temperature the observed temperature-independence of the crystallization of vortex lattices in BECs [106] and the decay of vortex tangles in Helium II [259, 86] has indicated that vortices are subject to a significant *dynamical* dissipation mechanism. Several theoretical works have suggested sound emission from the vortices as the decay process [87, 88, 90, 260, 261].

Due to the axis of rotation and well-ordered structure, the vortex dynamics in a lattice tend to be polarised in the direction of the axis, and dominated by rotational effects between vortices of the same topological charge. Vortex tangles, on the other hand, are disordered and have no preferred axis. As well as vortex lines, vortex rings are expected to form and play a major role in the dynamics [80]. The vortex dynamics in the tangle can take many forms; as well as rotational effects between adjacent vortex lines with the same topological charge, vortex lines and rings can collide and reconnect. Under reconnections, long-wavelength helical waves, known as Kelvin waves, can be excited along the vortex line. All of these dynamical effects are expected to induce decay in the

vortices via the emission of sound waves [87, 88, 149].

Due to its microscopic nature, the GPE is computationally demanding, and a full 3D description of a large system involving many vortices is currently unrealistic. One method of tackling the problem of many-vortex interactions on a microscopic level is to build up our understanding from cases involving a few vortices. In this chapter we consider the basic interactions between two and three vortices in a homogeneous system. We assume that the vortices are rectilinear and solve the 2D GPE. We show that, apart from the case of a vortex-antivortex pair, the vortex dynamics are generally accelerative, and lead to a decay in the vortex energy via sound emission. Some of this work has been presented in [262].

8.1 Corotating vortex pair

We consider first the case of two closely-positioned singly-charged vortices in a 2D homogeneous system, where the circulations are *parallel*. The density and phase profile of a pair with separation $d \approx 3.5\xi$ is illustrated in figure 8.1. Due to the mutual interaction of their circulating velocity fields, the vortices rotate about a point halfway between the cores. This excitation, known as a *corotating pair* (or vortex-vortex pair), can be regarded as the lowest order vortex lattice. Note that the far-field phase profile of the corotating pair resembles a double-charged vortex, and this implies that the pair is a topological excitation.

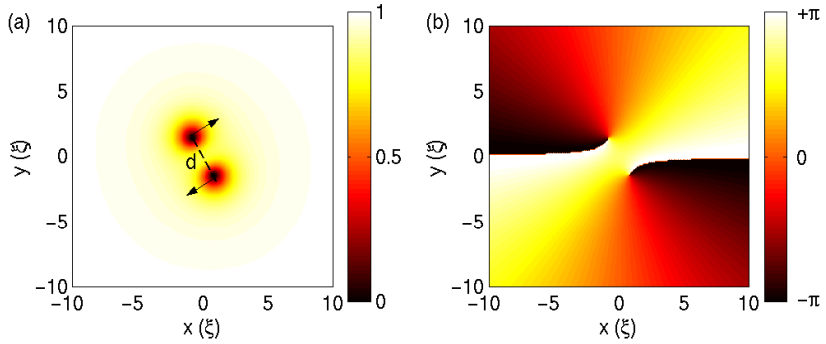

Figure 8.1: (a) Density and (b) phase of a corotating vortex pair in a 2D homogeneous system. The separation of the vortices is $d \approx 3.5\xi$.

8.1.1 Dynamical properties

The dynamical properties of the corotating vortex pair can be approximated using classical hydrodynamics [27, 149]. By assuming the vortices to be point-like, this approach ignores the core structure of the vortex, and so is only valid when the vortex cores are well separated. This approach predicts that the angular frequency of the corotating vortices is given by $\omega_{\mathrm{V}} = \kappa/\pi d^2$ [27, 153, 149], where d is the separation of the vortices and $\kappa = h/m$ is the quantum of circulation.

We can map the dynamics of the pair numerically by performing repeated simulations of the pair at different separations using the time-dependent 2D GPE. The angular frequency and acceleration of the corotating vortices are shown in figure 8.2 as a function of the vortex separation d. Here, data obtained from simulations of the time-dependent 2D GPE (points with error bars) is compared to the prediction based on classical hydrodynamics (dashed lines). As would be expected, the prediction agrees well with the time-dependent numerical results when the vortices are well separated, which roughly corresponds to separations greater than $d \sim 5\xi$. However, for separations smaller than this value we observe a significant deviation. Under the hydrodynamic predictions, both the angular frequency and acceleration diverge to infinity as the separation tends to zero. The numerical results suggest that, as the vortex separation is decreased, the angular frequency (figure 8.2(a)) gradually levels out, and for separations of less than $d \sim 2\xi$, reaches an approximately constant value of $\omega_{\mathrm{V}} \sim 0.25(c/\xi)$. Correspondingly, the numerically-obtained vortex acceleration (figure 8.2(b)) and speed (not shown) reach a peak at $d \sim 2\xi$ and decreases to zero as $d \to 0$. These effects at small separations are due to overlapping of the vortex cores. An important feature is that the numerical results suggest that there is a maximum acceleration and speed for an isolated corotating pair, approximately given by $a_{\mathrm{V}} \sim 0.06(c^2/\xi)$ and $v_{\mathrm{V}} \sim 0.25c$, respectively.

Also shown in figure 8.2 are numerical results based on the time-independent GPE in the rotating frame (solid lines)[263]. Despite the fact that the corotating pair is not a time-dependent solution to the GPE, the results are expected to be valid, and are found to be in reasonable agreement with the data obtained from the time-dependent 2D GPE.

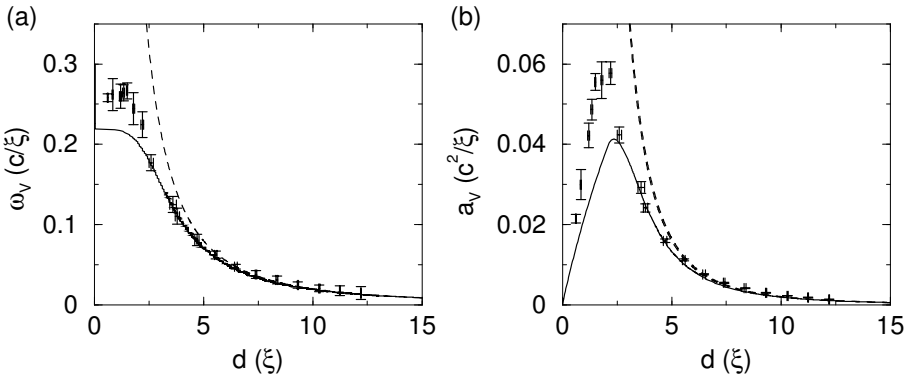

Figure 8.2: (a) Angular frequency ω_V and (b) acceleration a_V of a corotating pair as a function of the pair separation d. The results are derived from the (time-dependent) 2D GPE (points with error bars), a time-independent approach in the rotating frame (solid lines), and the hydrodynamical predictions corresponding to $\omega_V = \kappa/(\pi d^2)$ and $a_V = \kappa^2/(2\pi^2 d^3)$ [27, 149, 153] (dashed lines).

It has been predicted analytically that a superfluid corotating pair is dynamically unstable [149, 150, 151] and will decay via the continuous radiation of sound waves. The general form of the outgoing radiation is a summation over dipolar, quadrupolar, and higher order terms. Due to the symmetry of the corotating pair, the dipole fields from each vortex are expected to cancel such that the quadrupolar field dominates the radiation distribution [149, 150, 153].

Close examination of small-scale density perturbations in the region of the corotating pair during our time-dependent simulations reveals the continuous emission of sound waves from the vortices. This is illustrated in figure 8.3, which corresponds to figure 8.1(a) shown over a larger region and on a more sensitive density scale. As expected, the sound emission is clearly quadrupolar in nature. The rotation of the vortices modifies this quadrupolar emission into a swirling radiation pattern. We expect the quadrupolar radiation to have a frequency $2\omega_V$ [153]. For the pair considered here, with $d = 3.5\xi$, the angular frequency is $\omega_V \approx 0.14(c/\xi)$. We expect the wavelength of the emitted sound to be $\lambda = \pi c/\omega_V \approx 22\xi$, which is consistent with the appearance of the outgoing sound waves in figure 8.3. Note that the sound waves in figure 8.3 have a maximum amplitude of around $0.005n_0$, with the amplitude decreasing as the

waves spread radially outwards.

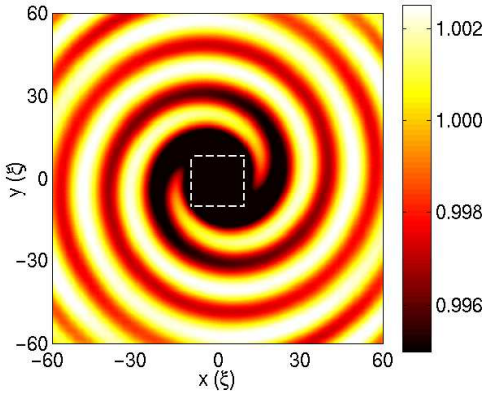

Figure 8.3: Density plot of the corotating pair considered in figure 8.1 showing small-scale density variations around the peak density. Sound waves of amplitude $\sim 0.5\% n_0$ are radiated from the pair in a quadrupolar manner, while the continuous rotation of the pair modifies the sound field into a swirling radiation pattern. Note that this figure is plotted on a larger length-scale than figure 8.1, the range of which corresponds to the white dashed box in this figure.

Since the system is homogeneous the core energy of the vortices cannot change, and so any energy loss must be at the expense of the interaction energy between the vortices. The interaction energy of the corotating pair depends on the vortex separation via $E_{\rm int} = -2\pi\kappa^2 \ln(d)$ [149]. The sound emission from the pair leads to a decrease in this interaction energy, and therefore causes the vortex separation to grow. Indeed, we observe this in the numerical simulations.

It has been predicted [149, 150, 151] that the rate of change of the separation is proportional to $1/d^5$, and the power emission is proportional to $1/d^6$. Note that, within this framework, the power emission from the pair is consistent with being proportional to the acceleration-squared. This decay is slow. For example, the vortex separation is expected to grow in time in proportion to $t^{1/6}$. For this reason, it is not computationally viable to map the decay of the pair using the time-dependent 2D GPE.

For more than two vortices in a symmetric circular configuration around some central axis, the quadrupolar radiation term disappears, and higher order terms dominate the radiation distribution. This leads to even slower decay rates than for the corotating pair [149].

8.2 Vortex-antivortex pair

If the circulation of the two vortices is in the opposite direction, the pair propagates with a constant, self-induced speed. This vortex-antivortex pair represents a solution to the homogeneous 2D GPE in the moving frame [208, 209], analogous to the non-stationary dark soliton solutions of the homogeneous 1D GPE. The vortex-antivortex pair can also be considered as the cross-section of a 3D vortex ring. Here we present some of the basic properties of the vortex-antivortex pair.

8.2.1 Dynamical properties

The density and phase profile of a vortex-antivortex pair is illustrated in figure 8.4 for a separation $d = 5\xi$. On a large density scale (figure 8.4(a)), two density minima can be resolved corresponding to the vortex cores. Examination of small-scale density perturbations about the peak density (figure 8.4(b)) reveals lobes of perturbed density in the plane of the pair and perpendicular to this along the axis of the pair. In the plane of the pair, the lobes are of reduced density due to the presence of vortex cores, while along the axis of the pair, the lobes are of slightly raised density. In the latter case, the lobes have a peak amplitude of $0.01n_0$ and extend over 10 healing lengths away from the vortex cores. The phase profile of the vortex-antivortex pair (figure 8.4(c)) is dipolar and tends towards a constant homogeneous phase with distance from the pair. In this sense, the vortex-antivortex pair is not a topological excitation.

Under the classical hydrodynamics approach [27], which is valid providing the vortices are well-separated, the velocity of the pair is predicted to be,

$$v_{\mathrm{P}} = \frac{\kappa}{2\pi d}. \tag{8.1}$$

Similarly the energy of the pair is predicted to be,

$$E_{\mathrm{P}} = \frac{n\kappa^2}{2\pi} \ln\left(\frac{d}{\xi}\right) + E_{\mathrm{P}}^0, \tag{8.2}$$

where the first term is the vortex kinetic energy and the second term E_{P}^0 is a constant representing the (rest mass) energy of the vortex cores. Figure 8.5 shows the total energy and speed of the vortex-antivortex pair as a function of separation, as computed numerically using the homogeneous 2D GPE (solid lines)

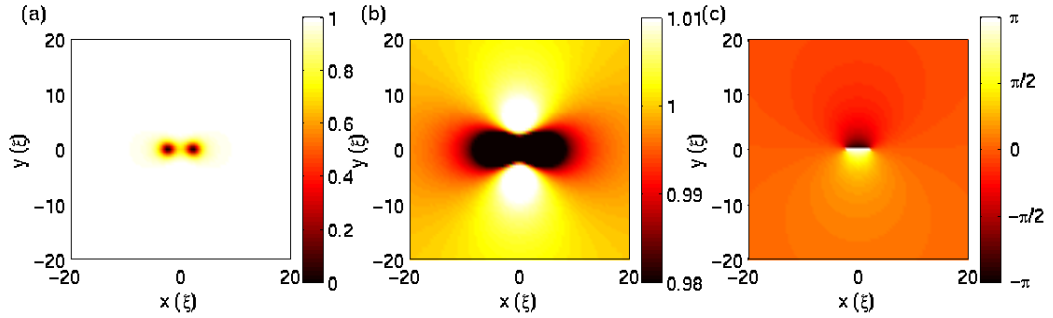

Figure 8.4: Density and phase profiles of a vortex-antivortex pair with separation $d = 5\xi$. (a) Large-scale density plot showing the two vortex cores. (b) Density plot on a small-scale revealing the quadrupolar lobe structure of the surrounding density, with amplitude $0.01n_0$. (c) Phase profile of the pair.

and the above predictions from classical hydrodynamics (dashed lines). As for the corotating pair, the hydrodynamical predictions agree well with the numerical data when the vortex separation is greater than $d \sim 5\xi$. For separations less than this, the predictions underestimate the numerically-obtained results. This is attributed to overlapping of the vortex cores, which is not described by classical hydrodynamics. Note that when the separation of the vortices is less than $d \sim 2\xi$, the pair is no longer stable and decays into a rarefaction pulse [208].

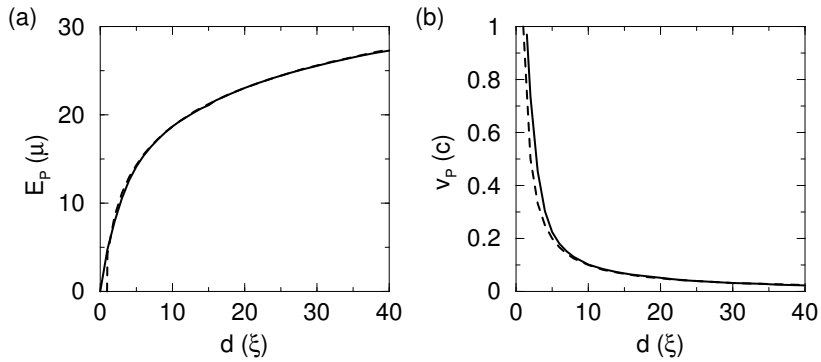

Figure 8.5: (a) Energy $E_{\rm P}$ and (b) speed $v_{\rm P}$ of the vortex-antivortex pair as a function of the separation d. The results obtained numerically from the 2D GPE are shown by solid lines, while the hydrodynamical predictions of equations (8.1)-(8.2) are shown by dashed lines. The energy term $E_{\rm P}^0$ in equation (8.2) is found by fitting to be $E_{\rm P}^0 \approx 4.25\mu$.

8.3 Interaction of a vortex-antivortex pair with a single vortex

As an example of a three-vortex interaction, we consider a vortex-antivortex pair incident on a single vortex in a 2D homogeneous system. The initial vortex configuration is illustrated schematically in figure 8.6(a). The vortex-antivortex pair, with vortices labelled 1 and 2, is created with its central point lying at the x-coordinate $x = h$. It is initially directed in the negative y-direction such that it approaches a single vortex, labelled 3, at the origin. Vortex 1 has clockwise circulation, while vortices 2 and 3 have anti-clockwise circulation. We investigate the dynamics of the three vortices during the ensuing interaction as a function of the initial offset h of the pair. The initial separation of the vortex-antivortex pair is $d = 5\xi$, while the initial y-coordinate of the pair is $y = 20\xi$.

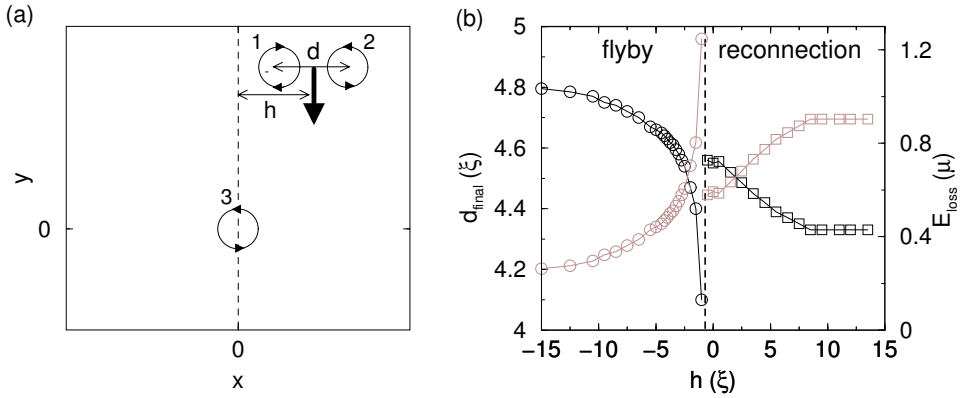

Figure 8.6: (a) Schematic of the three-body interaction. A vortex-antivortex pair, labelled 1 and 2, is incident on a single vortex, labelled 3, located at the origin. The initial offset of the pair from the $x = 0$ axis is h. (b) Final pair separation d_{final} (left axis, black data) and corresponding energy loss E_{loss} (right axis, grey data) for a pair with initial separation $d = 5\xi$ as a function of the offset distance h. The energy loss is inferred from the change in the pair separation, using equation (8.2), with the initial pair energy being $E_{\text{P}} = 14.4\mu$. Circles and squares denote the flyby and reconnection regimes, respectively.

We observe two regimes in the dynamics of the vortices: for $h \leq -\xi$, the vortex-antivortex travels past the single vortex with a deflected trajectory, while for $h \geq -0.5\xi$ a reconnection occurs whereby one of the vortices in the approaching

pair becomes swapped with the single vortex. We refer to these regimes as a *flyby* and a *reconnection*, respectively.

In a flyby interaction, vortex 2 in the pair is adjacent to vortex 3. These vortices have the same (anti-clockwise) circulation, and tend to repel each other. However, in the reconnective regime, the geometry of the interaction means that vortex 1 in the pair comes adjacent to vortex 3. These vortices have opposite charge, and can form a vortex-antivortex pair, leaving behind vortex 2. Note that we have simulated the reconnection events using smaller time/space steps, and can conclude that the reconnections are not numerical artifacts.

The decay of the vortex-antivortex pair during the interaction is mapped out in figure 8.6(b) by considering both the final pair radius (left axis, black data) and the corresponding energy loss (right axis, grey data). The left hand side of the plot ($h \leq \xi$) represents the flyby interaction, while the right hand side ($h \geq -0.5\xi$) represents the reconnection interaction. We will now make a detailed study of these two regimes in turn.

8.3.1 *Flyby* regime

The flyby regime occurs for $h \leq -\xi$. Figure 8.7(a) shows the trajectories of the vortices during the flyby interaction for several values of the offset distance h. The incoming pair, initially directed in the negative y-direction, becomes deflected by the velocity field of the single vortex. The single vortex makes slight deviations about its central position due to its interaction with the pair.

Dynamics of the vortices

The vortex pair tends to pass around the *far side* of the single vortex in an *anti-clockwise* sense. The amount of deflection depends heavily on how close the pair passes to the single vortex. For example, for the $h = -\xi$ case in figure 8.7(a) (blue lines), the pair experiences a strong circulating velocity field during the interaction due to its close proximity to the single vortex. This induces the pair to pass around the far side of the single vortex and almost reverse direction. Indeed, this pair becomes scattered by an angle $\sim 150^{\text{o}}$ in an anti-clockwise direction. As the initial offset h is increased in magnitude, the pair passes the

single vortex at a greater distance, reducing the velocity field it experiences, and therefore reducing the amount of deflection. For example, for $h = -4\xi$ in figure 8.7(a) (red case), the scattering angle is $\sim 30^o$ (anti-clockwise), while for $h = -12\xi$ (black case) the scattering is negligible.

During the flyby, the single central vortex makes small deviations about the origin due to its interaction with the pair. However it remains localised in the region of the origin at all times and returns to being stationary following the interaction.

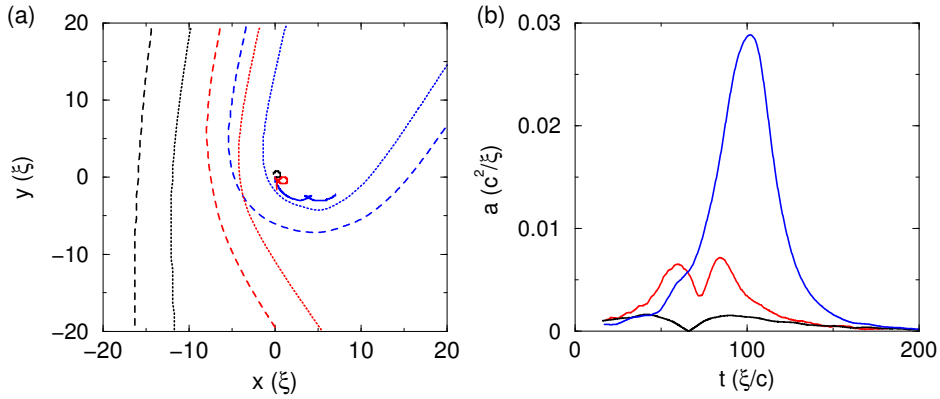

Figure 8.7: Dynamics of the vortices in the three-vortex interaction: flyby regime. (a) Path of the three vortices during their interaction, with vortices 1, 2 and 3 represented by dashed, dotted, and solid lines, respectively. Three values of the offset distance are considered: $h/\xi = -1$ (blue lines), -4 (red lines), and -12 (black lines). (b) Acceleration experienced by vortex 1 during the interactions considered in (a).

Energy loss during the flyby interaction

Since the system is homogeneous, the core energy of the vortices remains fixed, and the only energy contribution that can decay is the interaction energy of the vortex-antivortex pair. As evident from equation (8.2), the separation of the pair is a measure of its energy. In figure 8.6(b) we show the final separation of the pair (left axis, black data) following the interaction, as a function of the offset distance h. For the flyby regime (left side of figure8.6(b)), we observe that the *change* in separation is maximum for $h = -\xi$, and decreases asymptotically towards zero as $h \to \infty$. The maximum change in separation is almost 20% of

the original separation. Also plotted in figure 8.6(b) is the energy loss from the pair, derived from the change in the pair separation using equation (8.2). The maximum energy loss is $E_{\text{loss}} \sim 1.2\mu$, which corresponds to around 10% of the initial pair energy.

The amount of decay can be qualitatively understood in terms of the acceleration experienced by the pair. The pair acceleration is indicated in figure 8.7(b) for the three values of h considered in figure 8.7(a). Note that this acceleration corresponds to that of vortex 1, although this should have the same general form as the centre of mass acceleration of the pair. Due to the short-lived deflection of the pair by the single vortex, the acceleration consists of a peak, or double peak.

For $h = -\xi$ (blue data), where the deflection is considerable, the peak acceleration is of large amplitude. This corresponds to the case of maximum decay. For larger offsets, e.g. $h = -4\xi$ (red data) and $h = -12\xi$ (black data), the reduced deflections result in a much reduced peak acceleration. Correspondingly, the decay of the pair becomes reduced. In the limit $h \to \infty$, the acceleration and amount of decay both tend to zero.

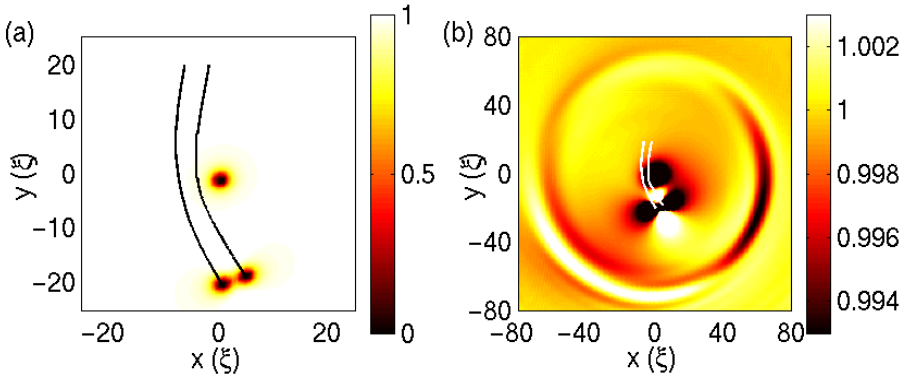

Figure 8.8: Density profile following the flyby interaction for initial offset $h = -4\xi$. (a) Density plot on a large density scale showing the position of the vortices at a time following the flyby interaction. (b) Density plot on a sensitive scale, revealing the emission of a burst of sound during the interaction. In both plots, the previous trajectory of the vortex-antivortex pair is indicated by solid lines. Note that (b) corresponds to a larger region than in (a).

We now address the question of what form the decay takes. We consider the case

for the offset $h = -4\xi$, corresponding to the red data in figure 8.7. Figure 8.8 shows the density profile in the region of the vortices following the interaction. In particular, figure 8.8(b) focusses on small-scale density perturbations. We observe the emission of a burst of sound from the interaction area, which propagates radially outwards. This sound pulse has an initial amplitude $\sim 0.5\% n_0$ and wavelength $\sim 20\xi$. The nature of this sharp (short wavelength) burst of sound is consistent with sharp acceleration experienced by the pair during the interaction (shown in figure 8.7(b), red line)).

8.3.2 *Reconnection* regime

For $h \geq -0.5\xi$, a vortex reconnection occurs. When the vortex-antivortex pair is in the vicinity of the central vortex, vortex 2 in the pair becomes replaced by the central vortex 3. This is possible since vortices 2 and 3 have the same circulation. Subsequently, vortex 2 becomes left behind in the region of the origin, and the new pair, consisting of vortices 1 and 3, propagates away.

Dynamics of the vortices

The paths of the vortices during the reconnective interaction are shown in figure 8.9(a) for several different initial offsets. The dynamics are more complicated than in the flyby regime, largely due to the effect of the reconnection.

For low h, e.g. $h = 0$ (blue lines), the outgoing pair becomes deflected anti-clockwise around the origin. Here, the swapping of vortex 2 and vortex 3 occurs over a short length-scale, and so the direction of motion of the pair just before and just after the reconnection is practically the same. In other words, the reconnection does not significantly affect the motion. The dominant effect on the motion of the pair is the velocity field of the central vortex - this induces an anti-clockwise motion of the pair around the single vortex, in a similar manner to that observed in the flyby regime.

As the offset h is increased, the anti-clockwise deflection of the pair decreases and eventually becomes clockwise, e.g. $h = 4\xi$ (red lines). This is due to the increasing effect of the reconnection on the pair dynamics. We find that the swapping of vortices 2 and 3 now occurs over a significant spatial extent. This

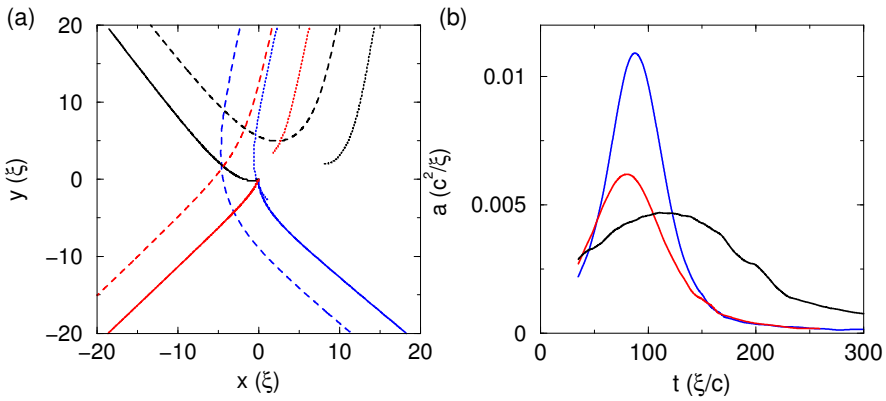

Figure 8.9: Dynamics of the vortices in the three-vortex interaction: reconnection regime. (a) Path of the vortices during the interaction, with vortices 1, 2 and 3 represented by dashed, dotted, and solid lines, respectively. Three values of the initial offset distance are considered: $h/\xi = 0$ (blue lines), 4 (red lines), and 12 (black lines). (b) Total acceleration experienced by all three vortices during the interactions considered in (a).

means that the orientation of the pair just before and just after the reconnection deviates, and induces a rapid *clockwise* change in the direction of motion.

For large offset, the spatial extent over which the vortices swap in the pair can be considerable. For $h = 12\xi$ (black lines in figure 8.9(a)), this distance is of the order of 10ξ. The corresponding scattering angle is $\sim 150^{\circ}$ in a clockwise manner.

Energy loss during the reconnection interaction

The decay of the vortex pair during the reconnective interaction is illustrated on the right side of figure 8.6(b). We find that the amount of decay in the pair increases with the initial offset distance h. However, for offsets greater than $h \sim 10\xi$, the decay appears to saturate. This maximum decay corresponds to a $\sim 14\%$ reduction in the pair separation and approximately 6% decay in the pair energy.

In order to investigate whether this decay trend is consistent with the acceleration experienced by the vortices, figure 8.9(b) shows the acceleration as a function of time, for offsets of $h/\xi = 0$ (blue line), 4 (red line), and 12 (black line). Due to the reconnection event, the acceleration of vortex 1 is not neces-

sarily a good indication of the overall vortex acceleration, so here we consider the summed acceleration of all three vortices.

Since the amount of pair decay increases with the offset h, we would expect to see a corresponding increase in the total acceleration experienced by the vortices. However, this is not the case. Firstly we note that the curves for $h = 0$ and $h = 4\xi$ are relatively sharp peaks, while for $h = 12\xi$ the acceleration is a broad peak due to the the relatively long-lived interaction. The area under the curves, representing the overall acceleration, is largest for $h = 0$ (blue line), smallest for $h = 4\xi$ (red line), while $h = 12\xi$ has an intermediate value. It is evident that the acceleration experienced by the vortices is not consistent with the decay of the pair.

These results are in contrast to the flyby regime, where the acceleration does give qualitative information about the decay. Therefore we expect that the process of reconnection must be responsible. It is known from studies of vortex rings that reconnections are accompanied by a substantial burst of sound emission [87]. Although a reconnection must involve some degree of accelerative motion, the amount of sound emitted is not necessarily directly dependent on it.

The form of the emitted energy from a reconnective interaction is illustrated in figure 8.10 by the density profile of the system following the interaction. We consider the case of $h = 0\xi$ (figure 8.9, red lines). Sound pulses are clearly radiated during the interaction, and appear to have a quadrupolar form. The sound pulse is broad, with a wavelength of around 60ξ, and of low initial amplitude $\sim 0.1\% n_0$. This is different to the sound emission observed in the flyby interaction of figure 8.8. There, the sound pulse appeared almost radial, with shorter wavelength and higher amplitude.

The flyby and reconnection regimes have distinct sound emission properties. In the former case, the accelerative motion induces the sound emission, whereas in the latter case, the reconnection is the dominant factor in generating sound. Importantly, when the acceleration of the vortices is large, e.g. in the regime $-2\xi < h < -0.5\xi$, the acceleration-induced sound emission can be significantly larger than that typically generated by a reconnection.

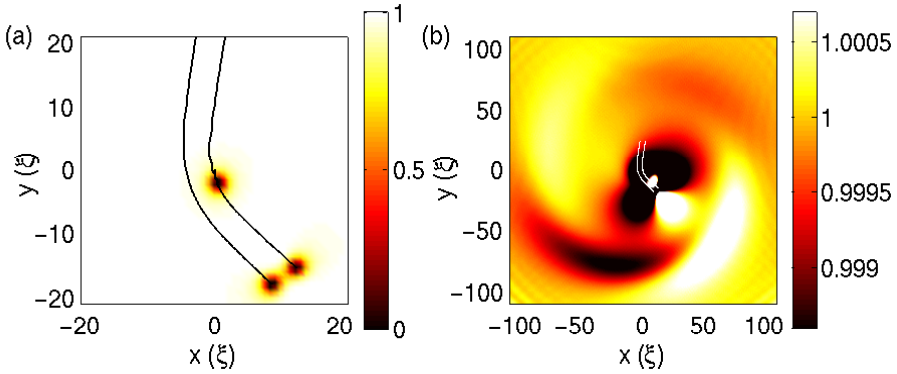

Figure 8.10: Density profile following the reconnective interaction for $h = 4\xi$. (a) Density plot on a large density scale, showing the position of the vortices at a time following the interaction. (b) Density plot on a senstive scale, revealing the emission of sound waves during the interaction. In both plots, lines indicate the previous trajectories of the vortices. Plot (b) corresponds to a larger region than plot (a).

8.4 Summary

In this chapter we have considered the interaction of two and three vortices in a 2D homogeneous system. Apart from the isolated vortex-antivortex pair, the dynamics of these vortex interactions are generally accelerative. We observe that this accelerative motion destabilises the vortices, and induces dissipation from the vortices via the radiation of sound waves. This is in qualitative agreement with the results of chapter 7 where we observed sound emission from a single accelerating vortex.

By considering the interaction of a vortex-antivortex pair with a single vortex, we have demonstrated reconnection events between vortices. A reconnection event results in a burst of sound waves from the vortices, in addition to the sound emission induced by the acceleration of the vortices.